

This Provisional PDF corresponds to the article as it appeared upon acceptance. Fully formatted PDF and full text (HTML) versions will be made available soon.

Interference alignment for spectral coexistence of heterogeneous networks

EURASIP Journal on Wireless Communications and Networking 2013,
2013:46 doi:10.1186/1687-1499-2013-46

Shree Krishna Sharma (shree.sharma@uni.lu)
Symeon Chatzinotas (symeon.chatzinotas@uni.lu)
Björn Ottersten (bjorn.ottersten@uni.lu)

ISSN 1687-1499

Article type Research

Submission date 29 June 2012

Acceptance date 31 January 2013

Publication date 22 February 2013

Article URL <http://jwcn.urasipjournals.com/content/2013/1/46>

This peer-reviewed article can be downloaded, printed and distributed freely for any purposes (see copyright notice below).

For information about publishing your research in *EURASIP WCN* go to

<http://jwcn.urasipjournals.com/authors/instructions/>

For information about other SpringerOpen publications go to

<http://www.springeropen.com>

© 2013 Sharma *et al.*

This is an open access article distributed under the terms of the Creative Commons Attribution License (<http://creativecommons.org/licenses/by/2.0>), which permits unrestricted use, distribution, and reproduction in any medium, provided the original work is properly cited.

Interference alignment for spectral coexistence of heterogeneous networks

Shree Krishna Sharma*¹

*Corresponding author

Email: shree.sharma@uni.lu

Symeon Chatzinotas¹

Email: symeon.chatzinotas@uni.lu

Björn Ottersten^{1,2}

Email: bjorn.ottersten@uni.lu

¹Interdisciplinary Centre for Security, Reliability and Trust (SnT), University of Luxembourg, 6 rue Richard Coudenhove-Kalergi, L-1359 Luxembourg-Kirchberg, Luxembourg

²Signal Processing Laboratory, KTH Royal Institute of Technology, SE-100 44 Stockholm, Sweden

Abstract

The coexistence of heterogeneous networks within the same spectrum for enhancing the spectrum efficiency has attracted large interest lately in the research community. Furthermore, the research interest towards the deployment of small cells and multibeam satellites is increasing due to high capacity, easier deployment and higher energy efficiency. However, due to the scarcity of available spectrum and the requirement of additional spectrum for these systems, small cells need to coexist with macrocells and multibeam satellites need to coexist with monobeam satellites within the same spectrum. In this context, this contribution investigates an underlay spectral coexistence mechanism which exploits an interference alignment (IA) technique in order to mitigate the interference of cognitive transmitters towards the primary receivers in a normal uplink mode. More specifically, three types of IA techniques, namely static, uncoordinated and coordinated are investigated. The performance of the IA technique is evaluated and compared with primary only, resource division and no-mitigation techniques in terms of sum-rate capacity, primary to secondary rate ratio and primary rate protection ratio. It is shown that the coordinated IA technique perfectly protects the primary rate in both terrestrial and satellite coexistence scenarios.

1 Introduction

Due to the limited and expensive spectrum resource, cognitive radio communication can be an efficient technique to enhance the spectrum efficiency in the context of coexistence of heterogeneous networks. Heterogeneous networks may exist within the same spectrum band in different ways such as two terrestrial networks or two satellite networks. In the terrestrial paradigm, the

coexistence of small cells and macrocells can be considered within the same spectrum while in the satellite paradigm the focus is on the coexistence of monobeam and multibeam satellite systems. Heterogeneous networks in this article refer to small/macro cell terrestrial and mono/multibeam satellite systems. In the context of terrestrial paradigm, the macrocell system can be considered as primary and a small cell system as secondary system. Similarly, in the context of dual satellite coexistence scenarios, a monobeam system can be considered as primary and a multibeam system as secondary. In both scenarios, the interference from the secondary system to the primary system should be suppressed while the secondary system must tolerate the interference from the primary system.

Due to the advancements in terrestrial cellular technology and satellite multibeam technology, denser deployments of cells/beams has become possible for providing higher capacity and network availability. Small cell systems provide higher cellular capacity and a large number of small cells is in general more energy efficient than macrocells since there is more flexibility of operating unused small cells in sleep mode due to their smaller coverage area [1]. Similarly, in satellite systems, multiple beams can be employed instead of a single global beam in order to enhance the capacity [2]. A geostationary satellite can be equipped with multibeam antennas to cover the multiple spots over the surface of the Earth. However, current network configurations use macrocell/monobeam systems and the deployment of new small cells/multibeam systems need additional bandwidth which is scarce and expensive to acquire. In this context, dense cellular networks (small cells) have to coexist with traditional macrocells and multibeam satellites have to coexist with the traditional monobeam satellites to utilize the existing spectrum optimally. This need has led to the concept of cognitive radio communications which allows for the coexistence of two systems, primary and secondary, over the same spectrum. The most common cognitive techniques in the literature can be categorized into spectrum sensing (SS) or interweave, underlay, overlay and database techniques [3]. In SS only techniques [4, 5], secondary users (SUs) are allowed to transmit whenever primary users (PUs) do not use that specific band, whereas in underlay techniques, SUs are allowed to transmit as long as they meet the interference constraint of the PUs.

The coexistence of heterogeneous networks in the same spectrum band can be modeled as cognitive radio networks with interference channels between primary and secondary systems. The operation of the primary network usually follows a well established standard and should not be degraded while the secondary network should employ advanced communication techniques to exploit the underutilized dimensions in the signal space. When the strength of secondary interference to the primary is comparable to the desired signal, treating as noise is not an option because of interference constraints while decoding and canceling requires complex primary receivers. In this context, interference alignment (IA) as an interference mitigation tool has received important attention recently in the cognitive radio research community [6, 7]. The concept behind IA is that signals can be designed in such a way that they cast overlapping shadows at the receivers where they constitute interference and remain distinguishable at the receivers where they are desired. In this direction, this study investigates an underlay spectral coexistence mechanism which exploits uplink interference alignment in order to mitigate the interference of small cell user terminals (UTs) towards the macrocell base station (BS) or the interference of multibeam satellite terminals towards the monobeam satellite. The proposed IA technique is compared to a passive transmission technique which allows for cochannel interference, as well as to a resource splitting approach which would require altering the spectrum

regulations. Furthermore, the performance of different IA techniques is evaluated in terms of ergodic sum-rate capacity, primary to secondary rate ratio and primary rate protection ratio.

The remainder of this article is structured as follows: Section 2 reviews in detail prior study in the areas of multicell/multibeam joint decoding and the IA technique. Section 3 describes the considered system models for terrestrial and satellite paradigms. Section 4 describes the considered signal model and channel model. Section 5 provides the capacity expressions and presents the proposed IA technique. Section 6 provides the considered performance metrics and evaluates the effect of various parameters on the system performance. Section 7 concludes the article.

1.1 Notation

Throughout this article, $\mathbb{E}[\cdot]$ denotes the expectation, $(\cdot)^\dagger$ denotes the conjugate transpose matrix, $(\cdot)^T$ denotes the transpose matrix, \odot denotes the Hadamard product and \otimes denotes the Kronecker product, \mathbf{I}_n denotes a $n \times n$ identity matrix, $\mathbb{I}_{n \times m}$ denotes a $n \times m$ matrix of ones, and $\mathbf{0}$ represents a zero matrix.

2 Preliminaries and related study

2.1 Multicell/multibeam joint decoding

The concept of global multicell joint decoding (MJD), also known as BS cooperation, was initially proposed in two seminal articles [8, 9]. The main assumption is the existence of a central processor which is interconnected to all the BSs through a backhaul of wideband, delayless and error-free links. In addition, the central processor is assumed to have perfect channel state information (CSI) about all the wireless links of the system. These assumptions enable the central processor to jointly decode the signals from all the UTs of the system. In this scenario, intercell interference is less important and multiuser interference dominates the overall system performance. In this context, it has been demonstrated in [10] that Rayleigh fading promotes multiuser diversity which is beneficial for the ergodic capacity performance. Subsequently, realistic path loss models and user distribution were investigated in [11, 12] providing closed form capacity expressions based on the cell size, path loss exponent and user spatial probability density function (p.d.f.). The beneficial effect of multiple input multiple output (MIMO) links was established in [13, 14], where a linear scaling with the number of BS antennas was proven.

Similarly, in multibeam joint processing, multiple users can be jointly processed by a single gateway and multiuser detection (MUD) is possible. In this context, a multiuser decoding algorithm has been presented in [15]. The capacity analysis of multibeam joint decoding over composite satellite channels has been carried out in [16]. Joint multiuser processing techniques for multibeam satellites for both forward link and return link have been investigated in [17]. The studies in [15, 18, 19] consider reverse link scenarios. Authors in [18] proposed an iterative multiuser decoding algorithm for the return link of multibeam satellites. Moreover, the return link of a multibeam satellite with Rician fading was analyzed in [19] under the framework of Wyner's Gaussian cellular multiple access channel.

2.1.1 *Interference alignment*

The IA technique was firstly proposed in [20] and channel capacity as well as degrees of freedom for the interference channel have been analyzed. This technique has been shown to achieve the degrees of freedom for a range of interference channels [21–23]. Its principle is based on aligning the interference on a signal subspace with respect to the non-intended receiver, so that it can be easily filtered out by sacrificing some signal dimensions. The advantage is that this alignment does not affect the randomness of the signals and the available dimensions with respect to the intended receiver. The disadvantage is that the filtering at the non-intended receiver removes the signal energy in the interference subspace and reduces the multiplexing gain. The fundamental assumptions which render interference alignment feasible are that there are multiple available dimensions (space, frequency, time or code) and that the transmitter is aware of the CSI towards the non-intended receiver. The exact number of needed dimensions and the precoding vectors to achieve interference alignment are rather cumbersome to compute, but a number of approaches have been presented in the literature towards this end [24–26]. It should be noted that the IA technique can be classified as an underlay cognitive radio technique [27] since it deals with interference mitigation towards the primary system in frequency coexistence scenarios.

The IA technique was also investigated in the context of cellular networks, showing that it can effectively suppress cochannel interference [26, 28–30]. More specifically, the downlink of orthogonal frequency division multiple access (OFDMA) cellular network with clustered multicell processing is considered in [30], where interference alignment is employed to suppress intracluster interference while intercluster interference has to be tolerated as noise. In addition, authors in [29] consider the uplink of a limited-size cellular system without MJD, showing that the interference-free degrees of freedoms (dofs) can be achieved as the number of UTs grows large. In the same context, authors in [31] employ IA as an uplink interference mitigation technique amongst cooperating BS clusters for Rayleigh channels. Coming back to small cells, the study in [32] extends [31] by assuming clusters of small cells which dictate the use of a Rician channel. Finally, the authors in [33] propose Vandermonde-subspace Frequency Division Multiplexing for the downlink in order to null out the interference of small cells towards primary macro users. In [34], the IA technique has been applied in the coexistence scenario of small cells and a macrocell.

The IA technique has also been investigated in multicarrier systems in different settings [30, 35–37]. A projection based IA technique including the concepts of signal alignment and channel alignment has been investigated in [35]. The IA technique for an interference network with the multicarrier transmission over parallel sub-channels has been tackled in [36]. The signal alignment for multicarrier code division multiple access (MC-CDMA) in two way relay systems has been studied in [37]. Despite various literature about IA in terrestrial cellular networks, only few studies have been reported about IA in satellite literature. The feasibility of implementing subspace interference alignment (SIA) in a multibeam satellite system has been studied in [38] and it has been concluded that the SIA using frequency domain is advantageous for a multibeam satellite.

3 System model

We consider two different system models in terrestrial and satellite paradigms. Although these two systems have different characteristics and channel models, they can be studied using the same input-output equations as described in the signal model section. Furthermore, both systems operate in a normal uplink mode with the primary system as a single-user uplink and the secondary system as a multiuser uplink.

3.1 Macrocell and small cells

Let us consider a coverage area where a single macrocell operates receiving signals from a set of PUs. A number of small cells (N) operate over the same coverage area receiving signals from a set of SUs. Furthermore, the small cells are able of cooperating through a broadband backhaul (e.g., radio over fiber) and jointly decoding the received signals. After scheduling, we consider that for a single slot one macro UT and N small cell UTs are transmitting simultaneously over a common set of frequencies (Figure 1). Since the macrocell system is primary, interference coming from the small cell UTs has to be suppressed. On the other hand, the interference of the macro UT towards the small cell access points (APs) has to be tolerated as the small cell system is secondary. We consider all receivers and transmitters to be equipped with M multiple antennas. More specifically, the macro UT has M antennas while the BS, small cell UTs and the AP have $L = M + 1$ antennas. In order to suppress the interference caused by the small cell UTs, we assume that they have channel state information (CSI) towards the macro BS. This CSI can be easily measured if the small cell UTs are aware of the macrocell pilot signals.

Figure 1 System model, terrestrial coexistence scenario. Graphical representation of the considered cellular system model.

3.2 Monobeam and multibeam satellites

Let us consider one monobeam satellite (SAT1) and one multibeam satellite (SAT2) covering the same area as shown in Figure 2. It can be assumed that they communicate with different gateways. Monobeam satellite uses a single beam to provide coverage to the given area, whereas multibeam satellite uses several beams to provide coverage to the same area. From the perspective of spectral coexistence, we consider the monobeam system as primary and the multibeam system as secondary. In this aspect, the multibeam satellite has to tolerate the interference coming from the monobeam satellite terminal. However, the interference coming from multibeam satellite terminals towards the monobeam satellite has to be suppressed. In this aspect, the IA technique can be applied at the multibeam satellite terminals to mitigate the interference towards the primary satellite.

Figure 2 System model, satellite coexistence scenario. Graphical representation of the considered satellite system model.

We consider a single ST1, N number of ST2s served by N beams of SAT2. Multibeam joint processing is considered at the gateway of SAT2 to decode the received signals from ST2s jointly. Since a single gateway is responsible for processing the transmitted and received signals corresponding to a large geographic area, the application of joint processing techniques in the satellite context is centralized. After scheduling, we consider that one ST1 and N number of ST2s are transmitting simultaneously in a single slot over a common spectrum band. In this context, we consider spatial multiplexing for the primary monobeam system and we employ multiple dimensions (carriers) in the secondary multibeam system to align interference with the reference vector.

Furthermore, we consider that all the satellite terminals use multicarrier transmission scheme and the IA is employed at the ST2s over $L = M + 1$ carriers, affected by Adjacent Carrier Interference (ACI). In this context, we consider a narrowband frequency division multiple access (FDMA) system which can be applicable for L/S band mobile satellite systems. We consider that M number of symbols are transmitted by ST1 and 1 symbol per ST2 is transmitted by spreading across all the carriers. Furthermore, it should be noted that ST1 sends M symbols over M subcarriers whereas each ST2 sends 1 symbol over L subcarriers. To suppress the interference caused by ST2s using IA technique, CSI towards the SAT1 is required and we assume that this CSI can be acquired at the ST2s by listening to the pilot signals broadcasted from the gateway. In this context, we assume time division duplex (TDD) mode of operation and for a satellite system with frequency division duplex (FDD) mode of operation, an alternative way of acquiring CSI should be investigated since uplink CSI can not be derived from the downlink pilots in FDD mode. As an example, for satellite scenarios where FDD is used, the uplink CSI can be derived from uplink pilots and then can be fed back with the help of a gateway.

3.3 Discussion

In the considered terrestrial system model, small cell UTs are secondary transmitters (STs), small cell APs are Secondary Receivers (SRs), a macro UT is a primary transmitter (PT) and a macro BS is a primary receiver (PR). Similarly, in the satellite system model, the monobeam satellite SAT1 is the PR, the feeders of multibeam satellite SAT2 are the SRs, the multibeam satellite terminals ST2s are the STs and the monobeam satellite terminal ST1 is the PT.

In addition to CSI, STs and the PR should be aware of predefined IA vector \mathbf{v} to perform IA. Depending on how \mathbf{v} is calculated, we consider three different IA techniques: static, coordinated, and uncoordinated in our analysis. These techniques depend on the level of coordination between primary and secondary systems. The concept behind cognitive interference alignment is to employ precoding at the STs so that the received secondary signals at the PR are all aligned across the alignment vector \mathbf{v} . In this way, interference can be filtered out by sacrificing one degree of freedom and some part of the desired received energy. For this purpose, the PT utilizes only M out of L dofs and reserves one dof which is devoted to IA filtering. However, after filtering the signal is interference free and can be easily decoded using conventional detection techniques. The term cognitive comes from the fact that the STs have to be aware of the CSI and the vector \mathbf{v} to perform the precoding. On the other hand, the PR needs only to perform filtering adapted to vector \mathbf{v} and no additional awareness or intelligence is required. The only difference between considered satellite and terrestrial models is that in the terrestrial scenario, IA is over the spatial dimensions and in the satellite scenario, IA is over the subcarriers. A

common signal model can be used for both cases with different channel models as described in the following section.

4 Signal model

The received signal at the PR (primary link) is:

$$\mathbf{y}_1 = \mathbf{H}\mathbf{x} + \sum_{i=1}^N \mathbf{F}_i \mathbf{x}_i + \mathbf{z}_1, \quad (1)$$

where \mathbf{y}_1 is the $L \times 1$ received symbol vector, \mathbf{x} is the $M \times 1$ transmitted symbol vector from the PT, \mathbf{x}_i is the $L \times 1$ transmitted symbol vector from the i th ST and \mathbf{z}_1 is the receiver noise. All inputs \mathbf{x}, \mathbf{x}_i are assumed to be Gaussian and obey the following sum power constraints: $\mathbb{E}[\mathbf{x}^\dagger \mathbf{x}] \leq \gamma_{ps} M$ and $\mathbb{E}[\mathbf{x}_i^\dagger \mathbf{x}_i] \leq \gamma_{ss} L$, γ_{ps} being the transmit SNR^a of the PT and γ_{ss} being the transmit SNR of the ST. The $L \times M$ matrix \mathbf{H} represents the channel gains between the PR and the PT while the $L \times L$ matrix \mathbf{F}_i represents the channel gains between the PR and i th ST.

To simplify notations, we group all \mathbf{F}_i into a single $L \times NL$ matrix $\mathbf{F} = [\mathbf{F}_1 \dots \mathbf{F}_N]$. The received signal at the joint processor of the SRs (secondary link) is:

$$\mathbf{y}_2 = \sum_{i=1}^N \tilde{\mathbf{F}}_i \mathbf{x}_i + \tilde{\mathbf{H}}\mathbf{x} + \mathbf{z}_2, \quad (2)$$

where \mathbf{y}_2 is the $NL \times 1$ received symbol vector and \mathbf{z}_2 is the receiver noise. The $NL \times M$ channel matrix $\tilde{\mathbf{H}}$ represents the channel gains between all SRs and the PT while the $NL \times L$ channel matrix $\tilde{\mathbf{F}}_i$ represents the channel gains between all SRs and the i th ST. To simplify notations, we group all $\tilde{\mathbf{F}}_i$ into a single $NL \times NL$ matrix $\tilde{\mathbf{F}} = [\tilde{\mathbf{F}}_1 \dots \tilde{\mathbf{F}}_N]$.

4.1 Channel model for terrestrial coexistence

The considered channel model is based on a MIMO Rayleigh channel whose power is scaled according to a power-law path loss model (i.e., asymmetric power levels). More specifically,

$$\mathbf{H} = \alpha \mathbf{G}, \quad (3)$$

where α is the path loss coefficient between the BS and the macro UT and \mathbf{G} is a $L \times M$ random matrix with complex circularly symmetric (c.c.s.) independent identically distributed (i.i.d.) elements representing Rayleigh fading coefficients. Similarly,

$$\mathbf{F}_i = \alpha_i \mathbf{J}_i, \quad (4)$$

where α_i is the path loss coefficient between BS and i th small-cell UT and \mathbf{J}_i is a $L \times L$ random matrix with i.i.d. c.c.s. elements representing channel coefficients between small-cell BS and the i th small-cell UT. As a result,

$$\mathbf{F} = (\boldsymbol{\alpha}^T \otimes \mathbb{I}_{L \times L}) \odot \mathbf{J}, \quad (5)$$

with $\boldsymbol{\alpha} = [\alpha_1 \dots \alpha_N]^T$ and \mathbf{J} is a $L \times NL$ random matrix with i.i.d. c.c.s. elements. In addition,

$$\tilde{\mathbf{H}} = (\boldsymbol{\beta} \otimes \mathbb{I}_{L \times M}) \odot \tilde{\mathbf{G}}, \quad (6)$$

where $\boldsymbol{\beta} = [\beta_1 \dots \beta_N]^T$ includes path loss coefficients between all APs and macro UT and $\tilde{\mathbf{G}}$ denotes a $NL \times M$ random matrix with i.i.d. c.c.s. elements. Similarly,

$$\tilde{\mathbf{F}}_i = (\boldsymbol{\beta}_i \otimes \mathbb{I}_{L \times L}) \odot \tilde{\mathbf{J}}_i, \quad (7)$$

where $\boldsymbol{\beta}_i$ contains the path loss coefficient between all APs and the i th small-cell UT and $\tilde{\mathbf{J}}_i$ represents a $NL \times L$ random matrix with i.i.d. c.c.s. elements. As a result,

$$\tilde{\mathbf{F}} = (\mathbf{B} \otimes \mathbb{I}_{L \times L}) \odot \tilde{\mathbf{J}}, \quad (8)$$

with $\mathbf{B} = [\boldsymbol{\beta}_1 \dots \boldsymbol{\beta}_N]$ and $\tilde{\mathbf{J}}$ is a $NL \times NL$ random matrix with i.i.d. c.c.s. elements.

4.2 Channel model for satellite coexistence

In this scenario, we consider a spectral coexistence network of multibeam and monobeam satellite systems with interference channels between them. Each transmitter/receiver node consists of a single antenna and uses multicarrier transmission so that the channels can be represented as diagonal matrices, where the diagonal entries correspond to the different sub-channels. The multicarrier model considered in this scenario differs from MIMO (spatial) channel matrix with full entries as considered in the terrestrial scenario.

Due to imperfect bandpass filters^b, weak copies of adjacent carrier signals may leak into the central carrier causing adjacent carrier interference. Therefore, we consider a multicarrier channel model with ACI. We assume that each carrier goes through independent flat-fading channels. The multi-carrier channel matrix with ACI for the i th satellite link for L number of carriers can be written as:

$$\mathbf{H} = \begin{bmatrix} h_1 & \sqrt{\rho}h_2 & \dots & 0 \\ \sqrt{\rho}h_1 & h_2 & \dots & 0 \\ 0 & \sqrt{\rho}h_2 & \dots & 0 \\ \vdots & \vdots & \vdots & \vdots \\ 0 & 0 & h_{L-1} & \sqrt{\rho}h_L \\ 0 & 0 & \sqrt{\rho}h_{L-1} & h_L \end{bmatrix}, \quad (9)$$

where ρ represents the fraction of carrier power leaked to adjacent carriers and the parameter h_i represents the Rician fading coefficient, given by;

$$h_i = \left(\sqrt{\frac{K}{K+1}}l + \sqrt{\frac{1}{K+1}}g_i \right), \quad (10)$$

where K is the Rician factor, l is a deterministic parameter representing the line of sight (LoS) component and g_i is a c.c.s. i.i.d. element for the i th satellite link representing the Rayleigh

fading coefficient. The channel matrix between the SAT1 and the i th ST2 can be written as:

$$\mathbf{F}_i = \alpha_i \mathbf{D}_i, \quad (11)$$

where α_i is the beam gain coefficient between the SAT1 and the i th SAT2 and \mathbf{D}_i has similar structure as \mathbf{H} . As a result,

$$\mathbf{F} = (\boldsymbol{\alpha}^T \otimes \mathbb{I}_{L \times L}) \odot \mathbf{D}, \quad (12)$$

with $\boldsymbol{\alpha} = [\alpha_1 \dots \alpha_N]^T$ and $\mathbf{D} = [\mathbf{D}_1 \dots \mathbf{D}_N]$. It is assumed that the fading coefficients are independent across block matrices \mathbf{D}_i . In addition, the channel matrix between SAT2 and the ST1 can be written as:

$$\tilde{\mathbf{H}} = (\boldsymbol{\beta} \otimes \mathbb{I}_{L \times M}) \odot \mathbf{P}, \quad (13)$$

where $\boldsymbol{\beta} = [\beta_1 \dots \beta_N]^T$ includes beam gain coefficients between SAT2 and the ST1 and $\mathbf{P} = [\mathbf{P}_1 \dots \mathbf{P}_N]^T$ is a block matrix with each \mathbf{P}_i having similar structure as \mathbf{H}^c . Similarly, the channel matrix between SAT2 and the i th ST2 can be written as:

$$\tilde{\mathbf{F}}_i = (\boldsymbol{\beta}_i \otimes \mathbb{I}_{L \times L}) \odot \mathbf{S}_i, \quad (14)$$

where $\boldsymbol{\beta}_i$ contains the beam gain coefficient between SAT2 and the i th ST2 and \mathbf{S}_i has similar structure as \mathbf{H} . As a result,

$$\tilde{\mathbf{F}} = (\mathbf{B} \otimes \mathbb{I}_{L \times L}) \odot \mathbf{S}, \quad (15)$$

with $\mathbf{B} = [\boldsymbol{\beta}_1 \dots \boldsymbol{\beta}_N]$ and the block matrix \mathbf{S} given by;

$$\mathbf{S} = \begin{bmatrix} \mathbf{S}_{11} & \mathbf{S}_{12} & \cdots & \mathbf{S}_{1N} \\ \mathbf{S}_{21} & \mathbf{S}_{22} & \cdots & \mathbf{S}_{2N} \\ & & \ddots & \\ \mathbf{S}_{N1} & \mathbf{S}_{N1} & \cdots & \mathbf{S}_{NN} \end{bmatrix}, \quad (16)$$

where each block \mathbf{S}_{ij} follows the similar structure as \mathbf{H} .

Higher gain can be achieved with a multibeam satellite in comparison to a monobeam satellite since each of the beams is narrower than a beam which would cover the whole of the region to be served. For the considered coexistence scenario, the monobeam and multibeam satellites can be adjacent or even collocated in terms of orbital slots. The beam gain of the satellite link in all the above cases are evaluated based on following expression [39]:

$$B(m, k) = G_T \cdot FL \cdot G_{\max} \cdot \left(\frac{J_1(u(m, k))}{2u(m, k)} + 36 \frac{J_3(u(m, k))^2}{u(m, k)^3} \right)^2, \quad (17)$$

where $B(m, k)$ represents the beam gain of k th beam for m th terminal position, $u(m, k) = 2.01723 \sin(\theta(m, k))/\theta_{3\text{dB}}$, J_i is the first kind of Bessel's function of order i , G_T is the terminal antenna gain, FL is the free space path loss for the satellite link, G_{\max} is the maximum satellite antenna gain, $\theta_{3\text{dB}}$ is the 3 dB angle and $\theta(m, k)$ represents the nadir angle to m th terminal position from k th beam center position with respect to the satellite position.

5 System performance

In this section, we provide the capacity expressions for different transmission techniques including proposed interference alignment technique and describe the different strategies for determining the alignment vector \mathbf{v} . Let us consider the following input-output relation for a MIMO system.

$$\mathbf{y} = \mathbf{H}\mathbf{x} + \mathbf{z} \quad (18)$$

with $\mathbb{E}[\mathbf{x}\mathbf{x}^\dagger] = \gamma\mathbf{I}$. The capacity of a MIMO channel is then given by [40];

$$C = \log \det (\mathbf{I} + \gamma\mathbf{H}\mathbf{H}^\dagger). \quad (19)$$

In the presence of cochannel interference, the input-output relation for a MIMO system can be written as:

$$\mathbf{y} = \mathbf{H}\mathbf{x} + \mathbf{H}_c\mathbf{x}_c + \mathbf{z} \quad (20)$$

with $\mathbb{E}[\mathbf{x}_c\mathbf{x}_c^\dagger] = \gamma_c\mathbf{I}$, where \mathbf{x}_c is a Gaussian vector transmitted by an interfering cochannel terminal. Then the capacity of a MIMO channel with input-output relation given by Equation (20) can be written as [41]:

$$C = \log \det (\mathbf{I} + \gamma_c\mathbf{H}\mathbf{H}^\dagger\mathbf{R}^{-1}), \quad (21)$$

where the term \mathbf{R}^{-1} includes the effect of cochannel interference and \mathbf{R} can be written as:

$$\mathbf{R} = \mathbb{E}[\tilde{\mathbf{z}}\tilde{\mathbf{z}}^\dagger] = \mathbf{I} + \gamma_c\mathbf{H}_c\mathbf{H}_c^\dagger \quad (22)$$

with $\tilde{\mathbf{z}} = \mathbf{H}_c\mathbf{x}_c + \mathbf{z}$. It should be noted that Equations (19) and (21) are used repeatedly in the following subsection to study the throughput of considered techniques.

5.1 Capacity expressions

5.1.1 Primary only

In this technique, we consider only the presence of a primary system and there is no interference from the secondary system. This case corresponds to current frequency allocations, according to which each band is allocated only to a primary system. For the considered system, the primary throughput can be written as:

$$C_{po} = \mathbb{E} \left[\log \det \left(\mathbf{I}_L + \frac{\gamma_{ps}}{M} \mathbf{H}\mathbf{H}^\dagger \right) \right], \quad (23)$$

where \mathbf{I}_L is the identity matrix of dimension L and γ_{ps} represents the SNR at the transmit antenna of the primary system.

5.1.2 Interference-limited

Assuming no interference mitigation and uniform power allocation across the multiple transmit antennas of the UTs and across the carriers of satellite terminals, the primary throughput can

be written as:

$$C_{ps} = \mathbb{E} \left[\log \det \left(\mathbf{I}_L + \frac{\gamma_{ps}}{M} \mathbf{H} \mathbf{H}^\dagger \left(\mathbf{I}_L + \frac{\gamma_{ss}}{L} \mathbf{F} \mathbf{F}^\dagger \right)^{-1} \right) \right], \quad (24)$$

where γ_{ss} represents the SNR at the transmit antenna of the secondary system. The secondary throughput with this technique can be written as:

$$C_{ss} = \mathbb{E} \left[\log \det \left(\mathbf{I}_{NL} + \frac{\gamma_{ss}}{L} \tilde{\mathbf{F}} \tilde{\mathbf{F}}^\dagger \left(\mathbf{I}_{NL} + \frac{\gamma_{ps}}{M} \tilde{\mathbf{H}} \tilde{\mathbf{H}}^\dagger \right)^{-1} \right) \right]. \quad (25)$$

In both cases, the second term represents the cochannel interference.

5.1.3 Resource splitting

In this technique, we assume that the available resource is split into two in order to allow the interference free parallel operation of primary and secondary systems. The orthogonalization can be done in time or frequency domain for the terrestrial scenario and in time domain for the satellite scenario. Although this is an impractical scenario since the primary system need to concede half of its spectrum, we consider this technique for the sake of completeness. The primary throughput with this technique can be written as:

$$\hat{C}_{pr} = \frac{1}{2} \mathbb{E} \left[\log \det \left(\mathbf{I}_L + \frac{2\gamma_{ps}}{M} \mathbf{H} \mathbf{H}^\dagger \right) \right] \quad (26)$$

while the secondary throughput can be written as:

$$\hat{C}_{sr} = \frac{1}{2} \mathbb{E} \left[\log \det \left(\mathbf{I}_{NL} + \frac{2\gamma_{ss}}{L} \tilde{\mathbf{F}} \tilde{\mathbf{F}}^\dagger \right) \right]. \quad (27)$$

5.1.4 Interference alignment

In this technique, interference alignment is employed at all the STs towards the PR and interference is filtered out at the PR by using the IA vector \mathbf{v} . The primary throughput in this case can be written as:

$$\bar{C}_{ps} = \mathbb{E} \left[\log \det \left(\mathbf{I}_M + \frac{\gamma_{ps}}{M} \bar{\mathbf{H}} \bar{\mathbf{H}}^\dagger \right) \right], \quad (28)$$

where $\bar{\mathbf{H}}$ is the equivalent channel matrix after IA filtering.

For the SRs, the interference coming from the PT has to be tolerated and thus secondary throughput can be written as:

$$\bar{C}_{ss} = \mathbb{E} \left[\log \det \left(\mathbf{I}_{NL} + \frac{\gamma_{ss}}{L} \bar{\mathbf{F}} \bar{\mathbf{F}}^\dagger \left(\mathbf{I}_{NL} + \frac{\gamma_{ps}}{M} \bar{\mathbf{H}} \bar{\mathbf{H}}^\dagger \right)^{-1} \right) \right], \quad (29)$$

where $\bar{\mathbf{F}}$ is the equivalent channel matrix including precoding.

5.2 Interference alignment and filtering

Let us assume a $L \times 1$ non-zero reference vector \mathbf{v} along which the interference should be aligned. It should be noted that STs are assumed to know the alignment direction \mathbf{v} and to have perfect own CSI about the channel coefficients \mathbf{F}_i towards the PR. As discussed in the next subsection, the alignment direction for each group of terminals can be predetermined or alternatively coordinated via signaling through the intended BS/gateway. In this context, the following precoding scheme is employed to align the interference:

$$\mathbf{x}_i = \mathbf{w}_i x_i = (\mathbf{F}_i)^{-1} \mathbf{v} v_i x_i, \quad (30)$$

where $\|\mathbf{v}\|^2 = L$ and $\mathbb{E}[\mathbf{x}_i^\dagger \mathbf{x}_i] \leq L\gamma$, the scaling variable v_i is needed to ensure that the input power constraint is not violated for each ST. This precoding results in unit multiplexing gain and is by no means the optimal IA scheme, but it serves as a tractable way of evaluating the IA performance. Following this approach, the cochannel interference can be expressed as:

$$\sum_{i=1}^N \mathbf{F}_i \mathbf{x}_i = \sum_{i=1}^N \mathbf{F}_i (\mathbf{F}_i)^{-1} \mathbf{v} v_i x_i = \mathbf{v} \sum_{i=1}^N v_i x_i. \quad (31)$$

It can be easily seen that interference has been aligned across the reference vector and it can be removed using a $M \times L$ zero-forcing filter \mathbf{Q} designed so that \mathbf{Q} is a truncated unitary matrix [22] and $\mathbf{Q}\mathbf{v} = \mathbf{0}$. After filtering, the $M \times 1$ received signal vector at the PR can be expressed as:

$$\bar{\mathbf{y}}_1 = \bar{\mathbf{H}}\mathbf{x} + \bar{\mathbf{z}}_1, \quad (32)$$

where $\bar{\mathbf{H}} = \mathbf{Q}\mathbf{H}$ is the $M \times M$ filtered channel matrix. Assuming that the system operates in high-SNR regime and is therefore interference limited, the effect of the AWGN noise coloring $\bar{\mathbf{z}}_1 = \mathbf{Q}\mathbf{z}_1$ can be ignored, namely $\mathbb{E}[\bar{\mathbf{z}}_1 \bar{\mathbf{z}}_1^H] = \mathbf{I}$. Furthermore, the received signal at the joint processor of the SRs (secondary link) is:

$$\bar{\mathbf{y}}_2 = \sum_{i=1}^N \bar{\mathbf{F}}_i x_i + \tilde{\mathbf{H}}\mathbf{x} + \mathbf{z}_2, \quad (33)$$

where $\bar{\mathbf{F}}_i = \tilde{\mathbf{F}}_i (\mathbf{F}_i)^{-1} \mathbf{v} v_i$ are the equivalent $NL \times 1$ channel matrices including precoding. To simplify notations we group all $\bar{\mathbf{F}}_i$ into a single $NL \times N$ matrix $\bar{\mathbf{F}} = [\bar{\mathbf{F}}_1 \dots \bar{\mathbf{F}}_N]$.

5.3 Alignment direction selection and filter design

In this section, we investigate various approaches for selecting the alignment direction \mathbf{v} and designing the corresponding filter \mathbf{Q} . Since these two operations are interdependent, they have to be jointly studied taking into account the level of coordination between the primary and secondary systems.

5.3.1 Static approach

In this approach, the alignment direction is predefined and does not depend on the channel state. It can be seen that this is quite static but also simple solution which assumes no coordination in the network. The disadvantage lies in the fact the IA direction may be aligned with one of the strong eigenvectors of the random PR-PT channel and in this case a large amount of received power will be filtered out.

5.3.2 Coordinated approach

This approach entails that the selection of the alignment direction takes place at the PR and is subsequently communicated to the STs. It is assumed that the channel coherence time is adequate for the alignment direction to be fed back and used by STs. This is an egoistic approach since the PR dictates the behavior of the STs in order to maximize the performance of the primary system. In this context, the following optimization problem can be defined:

$$[\mathbf{v}, \mathbf{Q}] = \arg \max_{\mathbf{v}, \mathbf{Q}} \bar{C}_{ps}, \quad \text{s.t. } \mathbf{Q}\mathbf{v} = 0, \mathbf{Q}\mathbf{Q}^\dagger = \mathbf{I}. \quad (34)$$

Now let $\mathbf{H}\mathbf{H}^\dagger = \mathbf{U}\mathbf{\Lambda}\mathbf{U}^\dagger$ be the eigenvalue decomposition of $\mathbf{H}\mathbf{H}^\dagger$ and $\lambda(\mathbf{H}\mathbf{H}^\dagger) = [0 \ \lambda_1 \ \dots \ \lambda_M]$ are the M ordered eigenvalues. The eigenvectors define an orthonormal space of the MIMO/multicarrier sub-channels. In this direction, the optimal strategy is to select the eigenvector which corresponds to the zero eigenvalue as the alignment direction.

Theorem 1 For $L = M + 1$, coordinated IA fully protects the primary rate, namely:

$$\bar{C}_{ps} = C_{po} \quad (35)$$

Proof 1 From Equations (23) and (28), it can be observed that the throughput for primary only technique is a function of eigenvalues of $\mathbf{H}\mathbf{H}^\dagger$ and the throughput for coordinated IA technique is a function of eigenvalues of $\bar{\mathbf{H}}\bar{\mathbf{H}}^\dagger$. The objective here is to show that both $\mathbf{H}\mathbf{H}^\dagger$ and $\bar{\mathbf{H}}\bar{\mathbf{H}}^\dagger$ have the same non-zero eigenvalues.

Since $\bar{\mathbf{H}} = \mathbf{Q}\mathbf{H}$, $\bar{\mathbf{H}}\bar{\mathbf{H}}^\dagger = \mathbf{Q}\mathbf{H}\mathbf{H}^\dagger\mathbf{Q}^\dagger$. Using the property $\det(\mathbf{I} + \gamma\mathbf{A}\mathbf{B}) = \det(\mathbf{I} + \gamma\mathbf{B}\mathbf{A})$, $\log \det \left(\mathbf{I}_M + \frac{\gamma_{ps}}{M} \bar{\mathbf{H}}\bar{\mathbf{H}}^\dagger \right) = \log \det \left(\mathbf{I}_M + \frac{\gamma_{ps}}{M} \mathbf{Q}^\dagger \mathbf{Q} \mathbf{H}\mathbf{H}^\dagger \right)$. Using eigenvalue decomposition, $\mathbf{Q}^\dagger \mathbf{Q}$ and $\mathbf{H}\mathbf{H}^\dagger$ can be written as: $\mathbf{Q}^\dagger \mathbf{Q} = \mathbf{V}\mathbf{B}\mathbf{V}^\dagger$, $\mathbf{H}\mathbf{H}^\dagger = \mathbf{U}\mathbf{\Lambda}\mathbf{U}^\dagger$, where \mathbf{U} and \mathbf{V} are unitary matrices. Hence,

$$\log \det \left(\mathbf{I}_M + \frac{\gamma_{ps}}{M} \mathbf{Q}^\dagger \mathbf{Q} \mathbf{H}\mathbf{H}^\dagger \right) = \log \det \left(\mathbf{I}_M + \frac{\gamma_{ps}}{M} \mathbf{V}\mathbf{B}\mathbf{V}^\dagger \mathbf{U}\mathbf{\Lambda}\mathbf{U}^\dagger \right) \quad (36)$$

Since \mathbf{Q} is truncated unitary, \mathbf{B} can be written as:

$$\mathbf{B} = \begin{bmatrix} 1 & 0 & \cdots & 0 & 0 \\ 0 & 1 & \cdots & 0 & 0 \\ & & \ddots & & \\ 0 & 0 & \cdots & 1 & 0 \\ 0 & 0 & \cdots & 0 & 0 \end{bmatrix} \quad (37)$$

and Λ is also a diagonal matrix with the following structure.

$$\Lambda = \begin{bmatrix} \lambda_M & 0 & \cdots & 0 & 0 \\ 0 & \lambda_{M-1} & \cdots & 0 & 0 \\ & & \ddots & & \\ 0 & 0 & \cdots & \lambda_1 & 0 \\ 0 & 0 & \cdots & 0 & 0 \end{bmatrix}, \quad (38)$$

where $\lambda_1, \lambda_2, \dots, \lambda_M$ corresponds to M eigenvalues. Using Property $\det(\mathbf{I} + \gamma\mathbf{AB}) = \det(\mathbf{I} + \gamma\mathbf{BA})$, Equation (36) can be written as:

$$\log \det \left(\mathbf{I}_M + \frac{\gamma_{ps}}{M} \bar{\mathbf{H}}\bar{\mathbf{H}}^\dagger \right) = \log \det \left(\mathbf{I}_M + \frac{\gamma_{ps}}{M} \mathbf{B}\mathbf{V}^\dagger\mathbf{U}\Lambda\mathbf{U}^\dagger\mathbf{V} \right). \quad (39)$$

Since truncated unitary matrix \mathbf{Q} in coordinated approach is constructed using the eigenvectors in \mathbf{U} , which correspond to non-zero eigenvalues, $\mathbf{V}^\dagger\mathbf{U}$ gives new unitary matrix $\tilde{\mathbf{V}}$ and has the following structure.

$$\mathbf{V}^\dagger\mathbf{U} = \begin{bmatrix} & & & 0 \\ & & & 0 \\ & \tilde{\mathbf{V}} & \vdots & \\ & & & 0 \\ 0 & 0 & \cdots & 0 & 1 \end{bmatrix} \quad (40)$$

After removing one dimension, Equation (39) can be written as:

$$\log \det \left(\mathbf{I}_M + \frac{\gamma_{ps}}{M} \mathbf{B}\mathbf{V}^\dagger\mathbf{U}\Lambda\mathbf{U}^\dagger\mathbf{V} \right) = \log \det \left(\mathbf{I}_M + \frac{\gamma_{ps}}{M} \mathbf{V}\tilde{\Lambda}\tilde{\mathbf{V}}^\dagger \right) = \log \det \left(\mathbf{I}_M + \frac{\gamma_{ps}}{M} \tilde{\Lambda} \right), \quad (41)$$

where $\tilde{\Lambda}$ contains the non-zero eigenvalues of $\mathbf{H}\mathbf{H}^\dagger$. Hence, $\bar{\mathbf{H}}\bar{\mathbf{H}}^\dagger$ and $\mathbf{H}\mathbf{H}^\dagger$ have identical eigenvalues in this approach and this completes the proof.

Remark 1 Due to the fact that we reserve one degree of freedom for interference alignment, the coordinated IA technique perfectly preserves the primary rate. Optimally there can be L data streams at primary transmitter and if we use all L degree of freedoms for signal transmission, there exists no zero eigenvalue and in that case, even the coordinated approach will have small gap as compared to the primary only technique.

5.3.3 Uncoordinated approach

This approach assumes that the primary and the secondary systems do not coordinate. Furthermore, STs are aware of their CSI towards the PR but have no information about the CSI of the PT. In this context, the STs have no other option than selecting an alignment direction which maximizes the secondary throughput. Subsequently, the PR is responsible for sensing the alignment direction and applying the appropriate filter. In this context, the following optimization problem can be defined:

$$[\mathbf{v}, \mathbf{Q}] = \arg \max_{\mathbf{v}, \mathbf{Q}} (\bar{C}_{ss}), \quad \text{s.t. } \mathbf{Q}\mathbf{v} = 0, \mathbf{Q}\mathbf{Q}^\dagger = 1. \quad (42)$$

Since the interference channel coefficients $\tilde{\mathbf{H}}$ are not known, we employ a simplified objective function:

$$[\mathbf{v}, \mathbf{Q}] = \arg \max_{\mathbf{v}, \mathbf{Q}} \text{trace}(\bar{\mathbf{F}}\bar{\mathbf{F}}^\dagger). \quad (43)$$

The solution of (43) is hard to tackle analytically. A heuristic solution for this problem would be to select the eigenvector corresponding to the largest eigenvalue of the equivalent channel covariance matrix $\sum_{i=1}^L \tilde{\mathbf{F}}_i (\mathbf{F}_i^{-1}) (\mathbf{F}_i^\dagger)^{-1} \tilde{\mathbf{F}}_i^\dagger = \mathbf{T}$. The matrix \mathbf{T} can be decomposed using the eigenvalue decomposition as: $\mathbf{T} = \mathbf{U}^\dagger \mathbf{\Lambda} \mathbf{U}$ with $\mathbf{U} = [\mathbf{u}_1, \mathbf{u}_2, \dots, \mathbf{u}_M]$ and $\mathbf{\Lambda}$ being a diagonal matrix with the eigenvalues in descending order. Therefore, one simple heuristic solution is to choose the eigenvector corresponding to the largest eigenvalue, i.e., $\mathbf{v} = \mathbf{u}_1$ and to design a truncated unitary matrix \mathbf{Q} so that the condition $\mathbf{Q}\mathbf{v} = 0$ is satisfied.

6 Numerical results

In this section, we present a number of numerical results in order to provide a comparative evaluation of the proposed technique. We consider two different simulation environments in satellite and terrestrial coexistence scenarios.

6.1 Performance metrics

In order to evaluate the system performance, three different metrics are considered. The system sum-rate capacity can be denoted by C_{sys} and is defined as:

$$C_{sys} = C_{ps} + \frac{C_{ss}}{N}, \quad (44)$$

where C_{ps} is the capacity of the primary system and C_{ss} is the sum-rate capacity of the secondary system. Subsequently, the primary to secondary rate ratio can be denoted by PSR and is defined as:

$$\text{PSR} = \frac{C_{ps}}{C_{ss}/N}. \quad (45)$$

Finally, the primary rate protection ratio can be denoted by PR and is defined as:

$$\text{PR} = \frac{C_{ps}}{C_{po}}. \quad (46)$$

6.2 Results and discussion

6.2.1 Terrestrial coexistence

While simulating the coexistence scenario in the terrestrial paradigm, a macro UT and small-cell UTs are considered to be uniformly distributed within the coverage area of the BS and the APs, respectively, as reflected in Figure 1. The APs are also uniformly distributed within the coverage area of the BS. We consider a MIMO channel with each component of the channel matrix being independent Rayleigh fading coefficient. The ergodic metrics are evaluated by averaging over a large number of channel realizations and positions. An overview of the parameter values and ranges used for producing the numerical results is presented in Table 1. For the static approach, we generate a random alignment vector at the beginning and keep it fixed for all the channel realizations. For the resource division approach, we consider resource sharing between the primary and secondary systems in the frequency domain^d as stated in Section 5.

Table 1 Parameters for capacity results in terrestrial paradigm

| Parameter | Symbol | Value | Range |
|----------------------------------|----------|-----------|-------|
| Number of small cells | N | | 1–10 |
| Macro UT antennas | M | 2 | |
| Small UT, BS, AP antennas | L | 3 | |
| Macrocell radius | R_{ps} | 2 Km | |
| Small cell radius | R_{ss} | 600 m | |
| Macro UT transmit power | P_{ps} | 0 dBW | |
| Small UT transmit power | P_{ss} | −6.02 dBW | |
| Path loss exponent | η | 3.5 | |
| Carrier bandwidth | | 5 MHz | |
| Number of Monte Carlo iterations | | 10^3 | |

Figure 3 presents the normalized system rate (C_{sys}) versus number of small cells (N) for the terrestrial coexistence scenario of small cells and the macrocell. From the figure, it can be observed that the sum-rate slowly increases with the value of N for all the considered techniques. The no-mitigation scheme achieves a three-fold gain while other techniques achieve a two-fold gain compared to primary only transmission. From this result, it seems that no-mitigation is promising but looking at the primary to secondary rate ratio in Figure 4, we can observe that this scheme does not perform well, especially for large values of N . The increased sum-rate for some techniques in Figure 3 is due to multiplexing gain in the primary system and applied multicell joint processing for the secondary system. Furthermore, it should be noted that total sum-rate capacity is the summation of primary sum-rate capacity and per beam secondary sum-rate and we apply the IA technique to get better spectral efficiency using the same frequency resource by primary and secondary systems.

Figure 3 Normalized system rate, terrestrial coexistence scenario. Normalized system rate versus number of small cells N .

Figure 4 Primary to secondary rate ratio, terrestrial coexistence scenario. Primary to secondary rate ratio versus number of small cells N .

Figure 4 presents the primary to secondary rate ratio versus N for different techniques. In general, the primary to secondary rate ratio decreases as more secondary small cells are included into the system. The IA techniques have the best performance with the coordinated approach ranking the first. This observation is further supported and verified by the primary rate protection ratio versus N plots in Figure 5. It should be especially noted that the coordinated IA technique fully protects the primary rate as expected, while other IA techniques preserve roughly 70% and the resource division preserves 82% of the primary rate. Furthermore, all techniques except no-mitigation preserve a constant protection rate with increasing N , while the performance of no-mitigation technique degrades monotonically.

Figure 5 Primary rate protection ratio, terrestrial coexistence scenario. Primary rate protection ratio versus number of small cells N .

6.2.2 Satellite coexistence

While simulating the coexistence scenario in the satellite paradigm, ST1 and ST2s are assumed to be uniformly distributed within the coverage area of the beams of SAT1 and SAT2, respectively, Figure 2. Furthermore, the beams of the multibeam antennas are also uniformly distributed within the coverage area of the monobeam satellite, emulating a beam hopping pattern. We consider a multicarrier channel model with ACI and each non-zero component of the channel matrix being independent Rician fading coefficient. The ergodic metrics are then evaluated by averaging over a large number of channel realizations and positions. Table 2 presents the parameter values and ranges used for producing the numerical results in this scenario. For the resource division approach in this context, we consider resource sharing between the primary and secondary systems in the time domain.

Figure 6 depicts the normalized system rate (C_{sys}) versus number of SAT2 beams N for different techniques and it can be observed that the coordinated IA technique performs better than all other techniques and the sum-rate slowly increases with N for this technique. The sum-rate for uncoordinated IA technique is worse than the coordinated IA technique and is still better than other considered techniques and it increases slowly with the value of N . Furthermore, the sum-rate for no mitigation technique decreases with the value of N , remains more or less constant with the value of N for resource division and remains constant for the primary only technique. The increased sum-rate capacity for the IA techniques is due to the combined effect of multibeam joint processing and the applied IA technique. The variation in the results in this scenario from the previous scenario is due to the different nature of the channel. In satellite coexistence scenario, the channel is non-zero mean and we consider a tridiagonal channel matrix with 3 correlated entries.

Table 2 Parameters for capacity results in satellite paradigm.

| Parameter | Symbol | Value | Range |
|---|------------|-----------------|--------|
| Number of ST2s | N | | 1 – 10 |
| Number of carriers used by ST1 | M | 4 | |
| Number of symbols transmitted by ST1 | | 4 | |
| Number of carriers used by ST2 | L | 5 | |
| Number of symbols transmitted by each ST2 | | 1 | |
| Monobeam radius | R_{ps} | 520 Km | |
| Multibeam radius | R_{ss} | 165 Km | |
| ST1 transmit power | P_{ps} | 10 dBW | |
| ST2 transmit power | P_{ss} | 3.98 dBW | |
| Receiver noise power @ 5 MHz | N_0 | -137 dBW | |
| Monobeam 3 dB beamwidth | BW_{ps} | 0.82° | |
| Multibeam 3 dB beamwidth | BW_{ss} | 0.26° | |
| Intercarrier interference component | ρ | 0.15 | |
| Rician factor | K | 12 dB | |
| Free space path loss | FL | 190 dB | |
| Max satellite antenna gain | G_{\max} | 48 dBi | |
| Terminal antenna gain | G_T | 5 dB | |
| Number of Monte Carlo iterations | | 10 ³ | |

Figure 6 Normalized system rate, satellite coexistence scenario. Normalized system rate versus number of SAT2 beams N .

Figure 7 shows the PSR versus N for different techniques. It can be observed that the maximum PSR is achieved with the coordinated IA technique and it decreases with the value of N . This happens due to the introduction of more number of beams in the considered coverage area. The PSR for IA uncoordinated, IA static and no-mitigation also decreases when more beams are introduced into the system. Furthermore, the PSR for the resource division technique increases slightly for lower values of N and remains constant at higher values of N . This is because the secondary throughput reduces with N due to the channel structure.

Figure 7 Primary to secondary rate ratio, satellite coexistence scenario. Primary to secondary rate ratio versus number of SAT2 beams N .

Figure 8 depicts the PR versus N plot for different techniques. It can be observed that the coordinated IA technique is optimal and matches with the primary only technique. This means that the coordinated IA technique fully protects the primary rate. Furthermore, all techniques except the no-mitigation technique shows a constant protection rate with the value of N , while the performance of no-mitigation decreases monotonically as in previous scenario. Moreover, the uncoordinated IA technique protects almost 90 % of the total primary rate and the resource division protects about 65 % of the total primary rate.

Figure 8 Primary rate protection ratio, satellite coexistence scenario. Primary rate protection ratio versus number of SAT2 beams N .

7 Conclusions

The spectral coexistence of heterogeneous networks in terrestrial and satellite paradigms has been investigated. The coexistence of small cells and macrocells equipped with MIMO transceivers in terrestrial paradigm and the coexistence of multibeam and monobeam satellites with multi-carrier transceivers in satellite paradigm have been considered. The primary only case has been compared to the coexistence scenarios with no mitigation, resource division and different IA techniques. More specifically, three types of IA have been considered depending on the level of network coordination and on whether it adapts to channel conditions. The different techniques have been compared in terms of system rate, primary to secondary rate ratio and primary rate protection rate. From the results, it can be deduced that the coordinated IA perfectly protects the primary rate. Although no mitigation achieves the highest sum-rate in terrestrial coexistence scenario, the primary protection rate degrades with the number of small cells. From the viewpoint of protecting primary rate as well as achieving the highest rate, the coordinated IA technique is the best among all other techniques in satellite coexistence scenario.

Endnotes

^aIn our signal model, we consider transmit SNR as the ratio of transmitted power to the noise variance.

^bThe main reason for ACI is due to imperfect bandpass filters since we consider a narrowband FDMA system in this study.

^cSince we consider transmission using M out of L carriers, excluding the last column from \mathbf{H} provides similar structure as \mathbf{P}_i .

^dIt is also possible to have resource division in time domain in this context.

Competing interests

The authors declare that they have no competing interests.

Acknowledgments

This study was supported by the National Research Fund, Luxembourg under Aids Training-Research (AFR) grant for PhD project (Reference 3069102) on “Spectrum Sensing, Resource Allocation and Resource Management Strategies for Satellite Cognitive Communications”, under the CORE project “CO2SAT: Cooperative and Cognitive Architectures for Satellite Networks” and by COST Action IC0902: “Cognitive Radio and Networking for Cooperative Coexistence of Heterogeneous Wireless Networks”.

References

1. B Badic, T O'Farrell, P Loskot, J He, in *IEEE 70th Vehicular Technology Conference (VTC 2009-Fall)*, Energy efficient radio access architectures for green radio: large versus small cell size deployment (Alaska, USA, 2009), pp. 1–5
2. S Chatzinotas, G Zheng, B Ottersten, in *IEEE Global Telecommunications Conference (GLOBECOM 2011)*, Joint precoding with flexible power constraints in multibeam satellite systems (Houston, Texas, 2011), pp. 1–5
3. SK Sharma, S Chatzinotas, B Ottersten, in *6th Advanced Satellite Multimedia Systems Conf. (ASMS) and 12th Signal Processing for Space Commun. Workshop (SPSC)*, Satellite cognitive communications: Interference modeling and techniques selection (Baiona, Spain, 2012), pp. 111–118
4. SK Sharma, S Chatzinotas, B Ottersten, in *7th Int. ICST Conf. on Cognitive Radio Oriented Wireless Networks and Communications (CROWNCOM)*, Exploiting polarization for spectrum sensing in cognitive SatComs (Stockholm, Sweden, 2012), pp. 36–41
5. SK Sharma, S Chatzinotas, B Ottersten, in *IEEE Global Communications Conf.*, Spectrum Sensing in Dual Polarized Fading Channels for Cognitive SatComs (Anaheim, California, 2012), pp. 3443–3448
6. H Zhou, T Ratnarajah, YC Liang, in *IEEE Symposium on New Frontiers in Dynamic Spectrum Access Networks (DySPAN)*, On secondary network interference alignment in cognitive radio (Aachen, Germany, 2011), pp. 637–641
7. S Kaimaletu, R Krishnan, S Kalyani, N Akhtar, B Ramamurthi, in *IEEE International Conference on Communications (ICC)*, Cognitive interference management in heterogeneous femto-macro cell networks (Kyoto, Germany, 2011), pp. 1–6
8. SV Hanly, PA Whiting, Information-theoretic capacity of multi-receiver networks. *Telecommun. Syst.* **1**, 1–42 (1993)
9. A Wyner, Shannon-theoretic approach to a Gaussian cellular multiple-access channel. *IEEE Trans. Inf. Theory* **40**(6), 1713–1727 (1994)
10. O Somekh, S Shamai, Shannon-theoretic approach to a Gaussian cellular multiple-access channel with fading. *IEEE Trans. Inf. Theory* **46**(4), 1401–1425 (2000)
11. S Chatzinotas, M Imran, C Tzaras, On the capacity of variable density cellular systems under multicell decoding. *IEEE Commun. Lett.* **12**(7), 496–498 (2008)
12. S Chatzinotas, MA Imran, C Tzaras, in *IEEE 9th Workshop on Signal Processing Advances in Wireless Communications (SPAWC'08)*, Optimal information theoretic capacity of the planar cellular uplink channel (Pernambuco, Brazil, 2008), pp. 196–200
13. D Aktas, M Bacha, J Evans, S Hanly, Scaling results on the sum capacity of cellular networks with MIMO links. *IEEE Trans. Inf. Theory* **52**(7), 3264–3274 (2006)
14. S Chatzinotas, MA Imran, C Tzaras, in *IEEE Int. Symposium on Wireless Communication Systems (ISWCS'08)*, Uplink capacity of MIMO cellular systems with multicell processing (Reykjavik, Iceland, 2008), pp. 453–457

15. ML Moher, Multiuser decoding for multibeam systems. *IEEE Trans. Veh. Technol.* **49**(4), 1226–1234 (2000)
16. D Christopoulos, S Chatzinotas, M Matthaiou, B Ottersten, in *Forty Fifth Asilomar Conference on Signals, Systems and Computers*, Capacity analysis of multibeam joint decoding over composite satellite channels (Pacific Grove, CA, USA, 2011), pp. 1795–1799
17. D Christopoulos, S Chatzinotas, G Zheng, J Grotz, B Ottersten, Linear and nonlinear techniques for multibeam joint processing in satellite communications. *EURASIP J. Wirel. Commun. Network.* **2012**(162) (2012)
18. M Debbah, G Gallinaro, R Müller, R Rinaldo, A Vernucci, in *9th International Workshop on signal processing for space communications*, Interference mitigation for the reverse-link of interactive satellite networks (Noordwijk, Netherlands, 2006)
19. N Letzepis, A Grant, Capacity of the multiple spot beam satellite channel with rician fading. *IEEE Trans. Inf. Theory* **54**(11), 5210–5222 (2008)
20. V Cadambe, S Jafar, in *IEEE International Conference on Communications (ICC)*, Interference alignment and spatial degrees of freedom for the K user interference channel (Beijing, China, 2008), pp. 971–975
21. V Cadambe, S Jafar, Interference alignment and degrees of freedom of the K-user interference channel. *IEEE Trans. Inf. Theory* **54**(8), 3425–3441 (2008)
22. V Cadambe, S Jafar, Interference alignment and the degrees of freedom of wireless X networks. *IEEE Trans. Inf. Theory* **55**(9), 3893–3908 (2009)
23. S Jafar, S Shamai, Degrees of freedom region of the MIMO X channel. *IEEE Trans. Inf. Theory* **54**, 151–170 (2008)
24. K Gomadam, V Cadambe, S Jafar, in *IEEE Global Telecommunications Conference*, Approaching the capacity of wireless networks through distributed interference alignment (New Orleans, LA, USA, 2008), pp. 1–6
25. CM Yetis, T Gou, SA Jafar, AH Kayran, On feasibility of interference alignment in MIMO interference networks. *IEEE Trans. Signal Process.* **58**(9), 4771–4782 (2010)
26. R Tresch, M Guillaud, E Riegler, in *IEEE/SP 15th Workshop on Statistical Signal Processing*, On the achievability of interference alignment in the K-user constant MIMO interference channel (Cardiff, United Kingdom, 2009), pp. 277–280
27. A Goldsmith, S Jafar, I Maric, S Srinivasa, Breaking spectrum gridlock with cognitive radios: an information theoretic perspective. *Proc. IEEE* **97**(5), 894–914 (2009)
28. S Chatzinotas, B Ottersten, in *IEEE Wireless Communications and Networking Conference*, Interference alignment for clustered multicell joint decoding (Quintana-Roo, Mexico, 2011), pp. 1966–1971
29. C Suh, D Tse, in *46th Annual Allerton Conference on Communication, Control, and Computing*, Interference alignment for cellular networks (Monticello, IL, USA, 2008), pp. 1037–1044

30. B Da, R Zhang, in *IEEE Global Telecommunications Conference*, Exploiting interference alignment in multi-cell cooperative OFDMA resource allocation (Houston, Texas, USA, 2011), pp. 1–5
31. S Chatzinotas, B Ottersten, Interference mitigation techniques for clustered multicell joint decoding systems. *EURASIP J. Wirel. Commun. Network. (Special Issue on Multicell Cooperation for Next Generation Communication Systems)* **132** (2011)
32. ATA Masucci, M Debbah, in *IEEE Global Telecommunications Conference*, Asymptotic analysis of uplink interference alignment in Ricean small cells (Houston, Texas, 2011)
33. M Maso, L S Cardoso, M Debbah, L Vangelista, in *IEEE 13th International Workshop on Signal Processing Advances in Wireless Communications (SPAWC)*, Cognitive interference alignment for OFDM two-tiered networks (Cesme, Turkey, 2012), pp. 244–248
34. S Chatzinotas, B Ottersten, in *19th International Conference on Telecommunications*, Cognitive interference alignment between small cells and a macrocell (Jounieh, Lebanon, 2012), pp. 1–6
35. R Ganesan, A Klein, in *8th International Symposium on Wireless Communication Systems*, Projection based space-frequency interference alignment in a multi-carrier multi-user two-way relay network (Aachen, Germany, 2011), pp. 266–270
36. C Shi, R Berry, M Honig, in *IEEE International Symposium on Information Theory Proceedings*, Interference alignment in multi-carrier interference networks (Saint Petersburg, Russia, 2011), pp. 26–30
37. T Liu, C Yang, Signal alignment for multicarrier code division multiple user two-way relay systems. *IEEE Trans. Wirel. Commun.* **10**(11), 3700–3710 (2011)
38. P Jain, M Vazquez-Castro, in *5th Advanced satellite multimedia systems conference and the 11th signal processing for space communications workshop*, Subspace interference alignment for multibeam satellite communications systems (Sardinia, Italy, 2010), pp. 234–239
39. M Diaz, N Courville, C Mosquera, G Liva, G Corazza, in *International Workshop on Satellite and Space Communications*, Non-linear interference mitigation for broadband multimedia satellite systems (Salzburg, Austria, 2007), pp. 61–65
40. A Lozano, A Tulino, Capacity of multiple-transmit multiple-receive antenna architectures. *IEEE Trans. Inf. Theory* **48**(12), 3117–3128 (2002)
41. R Blum, MIMO capacity with interference. *IEEE J. Sel. Areas Commun.* **21**(5), 793–801 (2003)

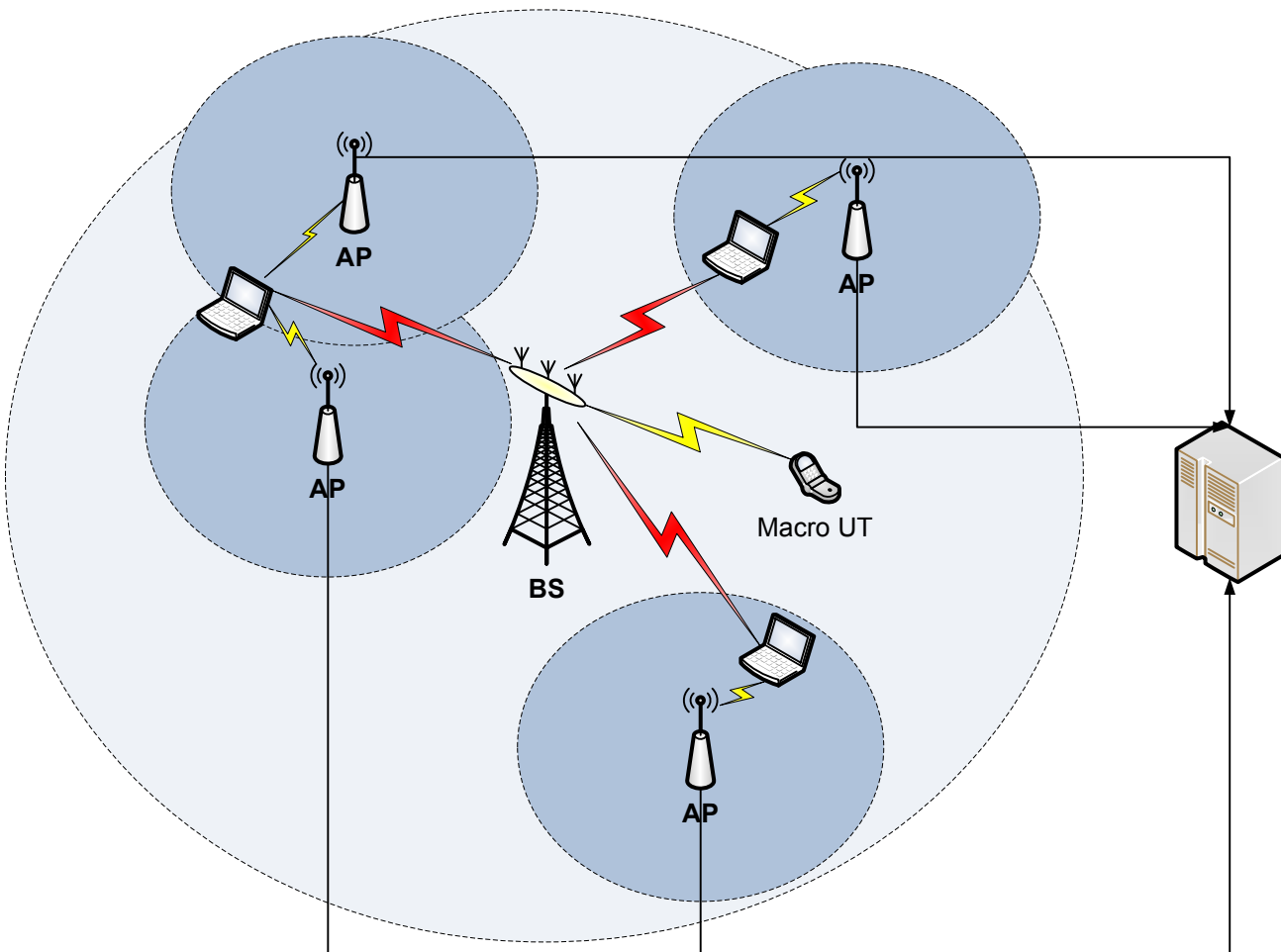


Figure 1

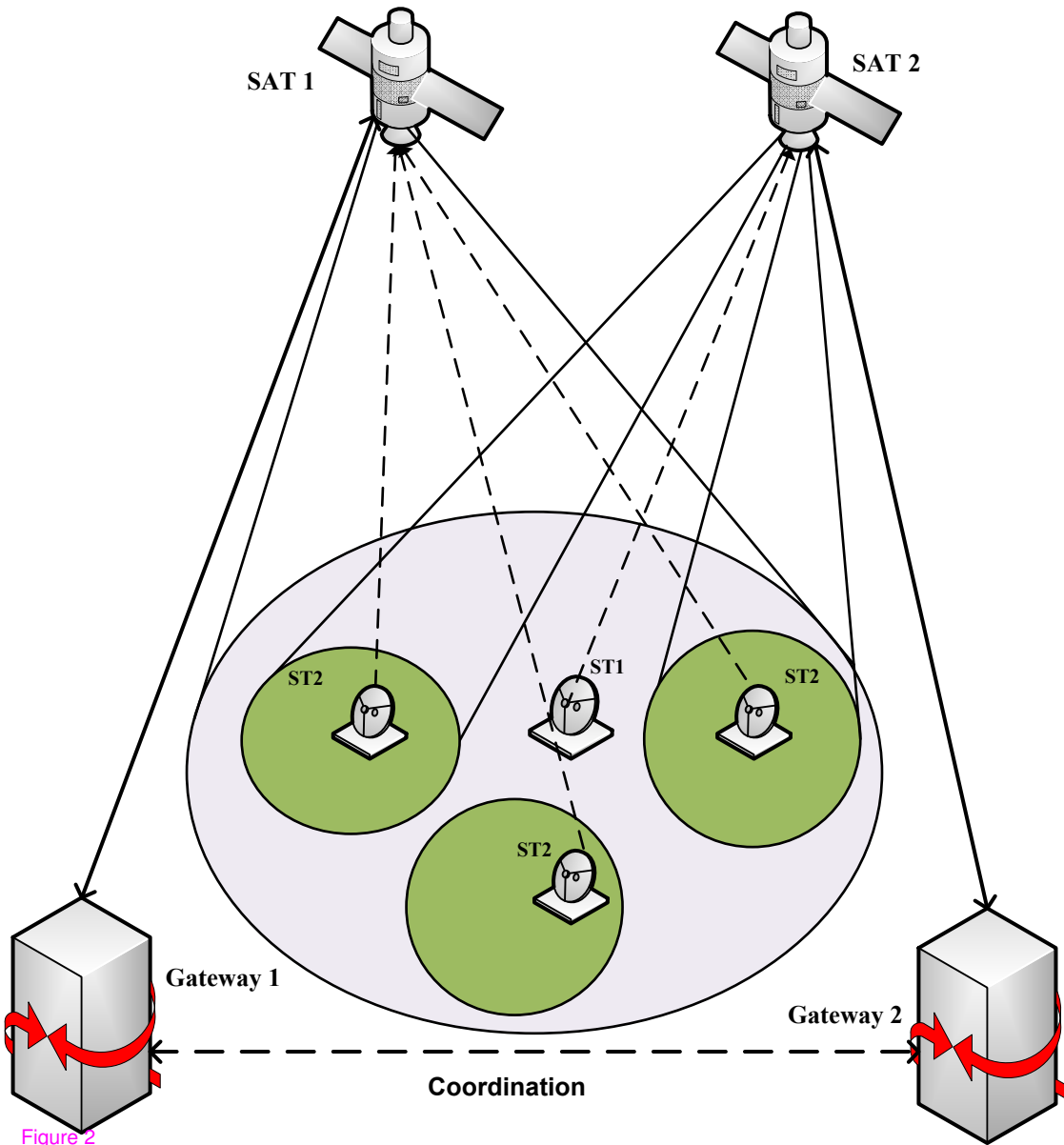


Figure 2

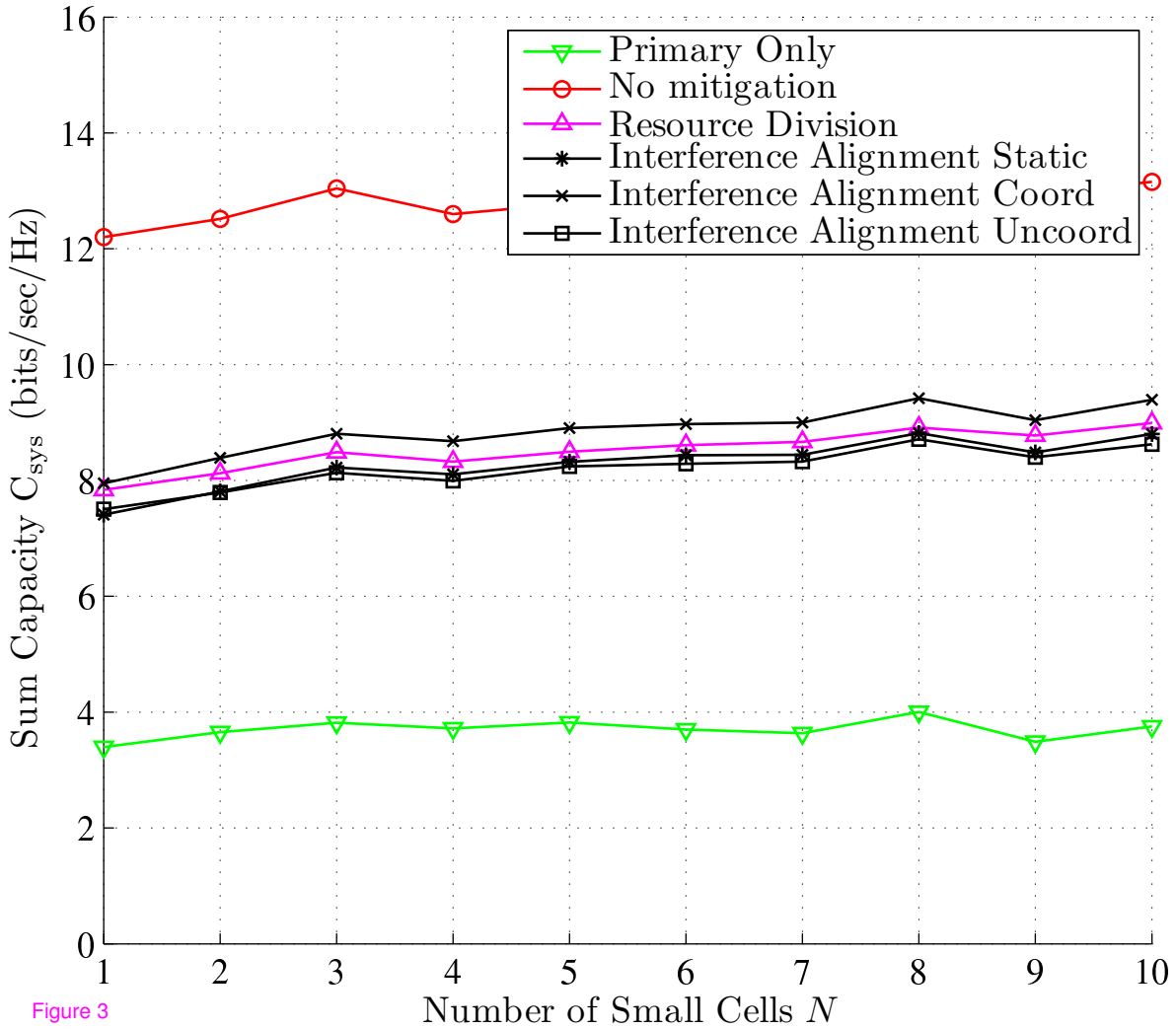
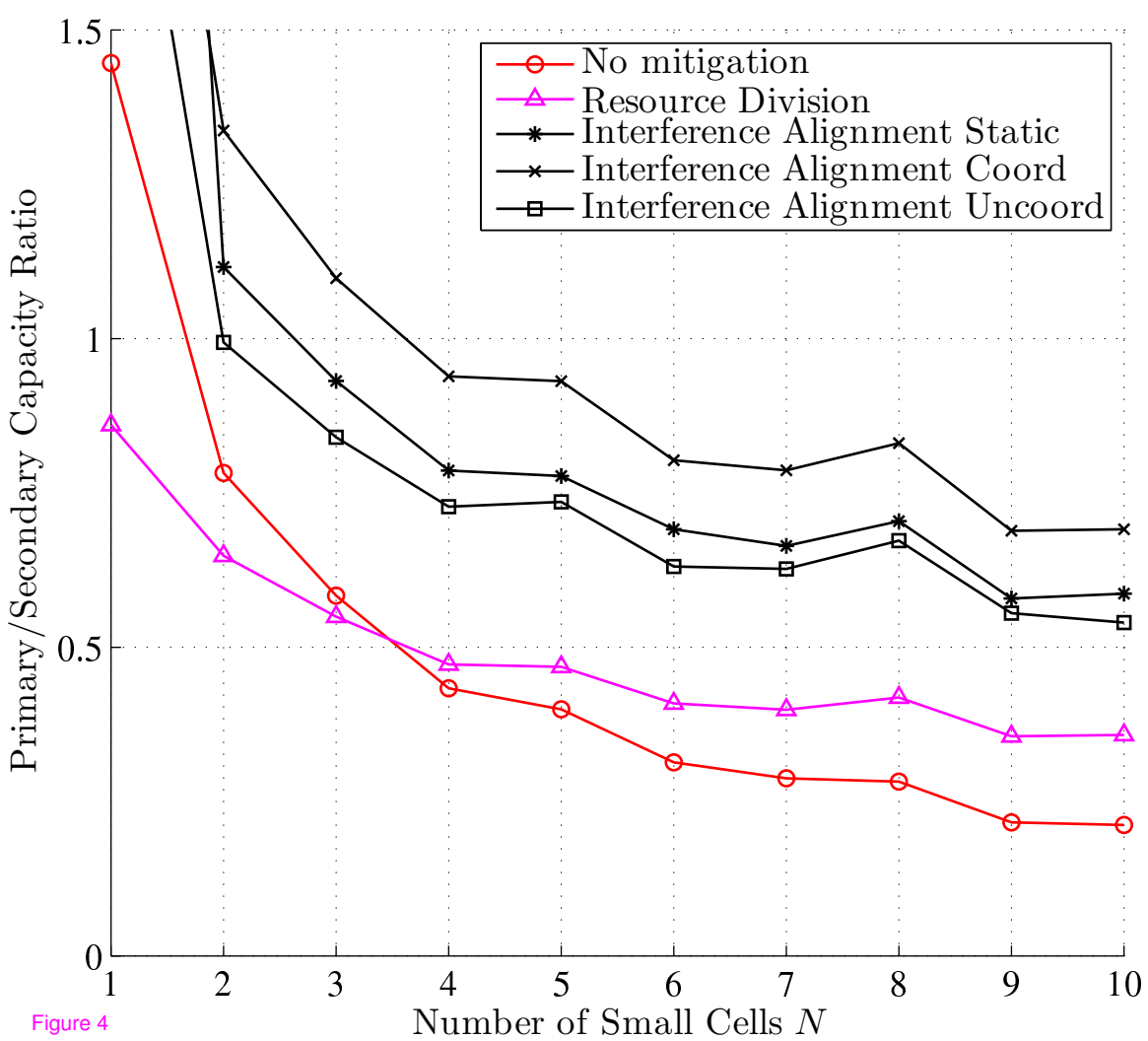


Figure 3



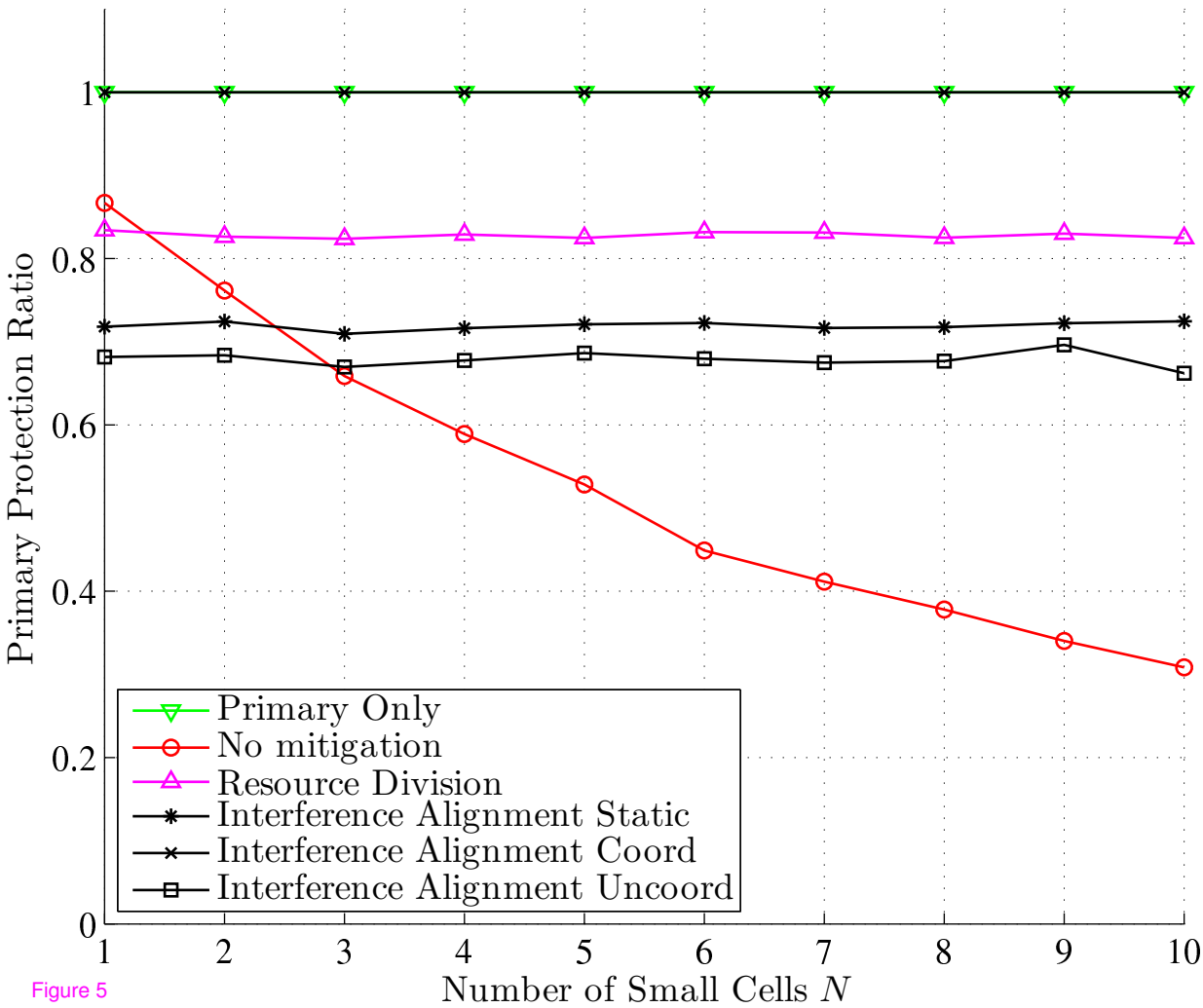


Figure 5

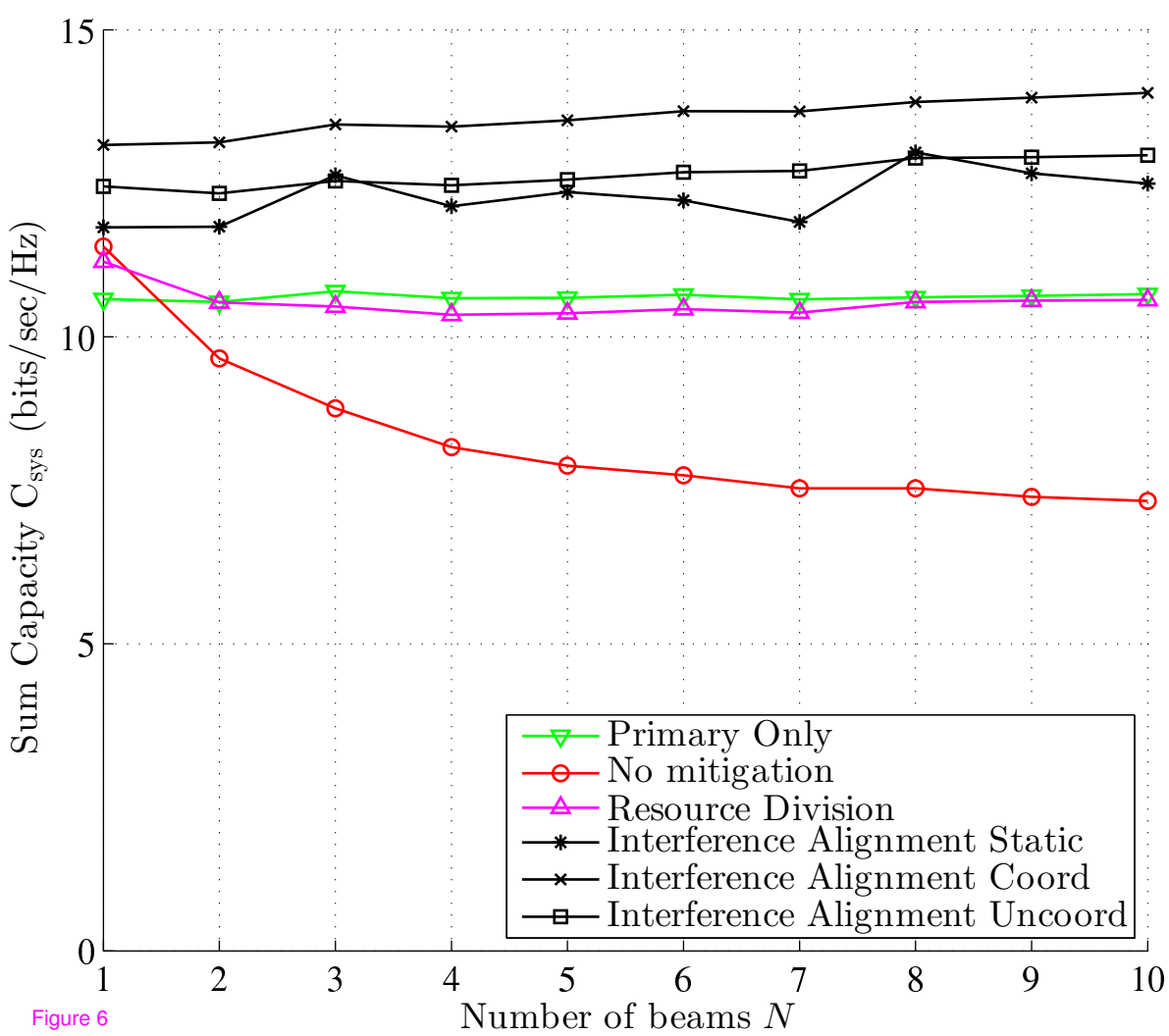


Figure 6

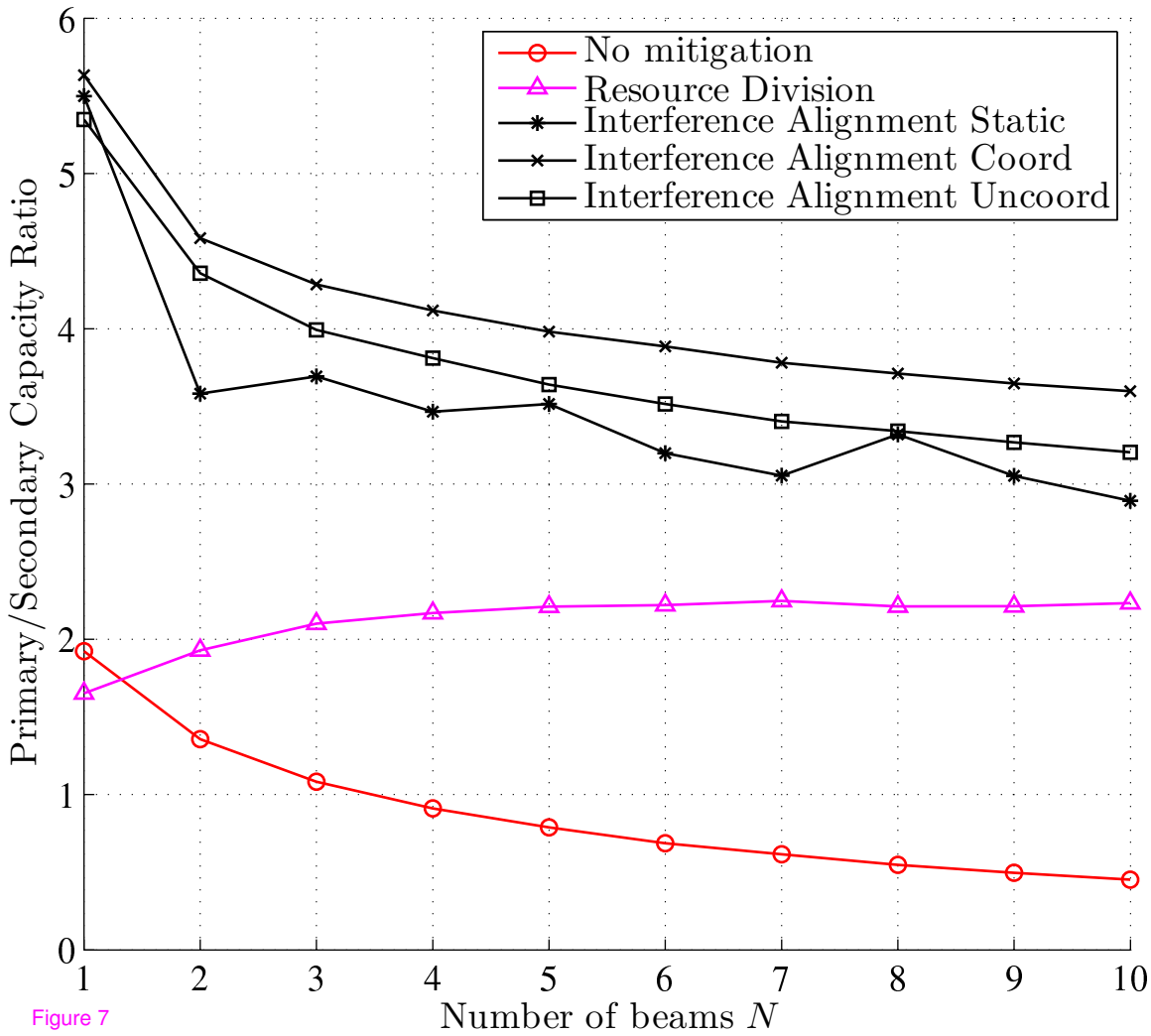


Figure 7

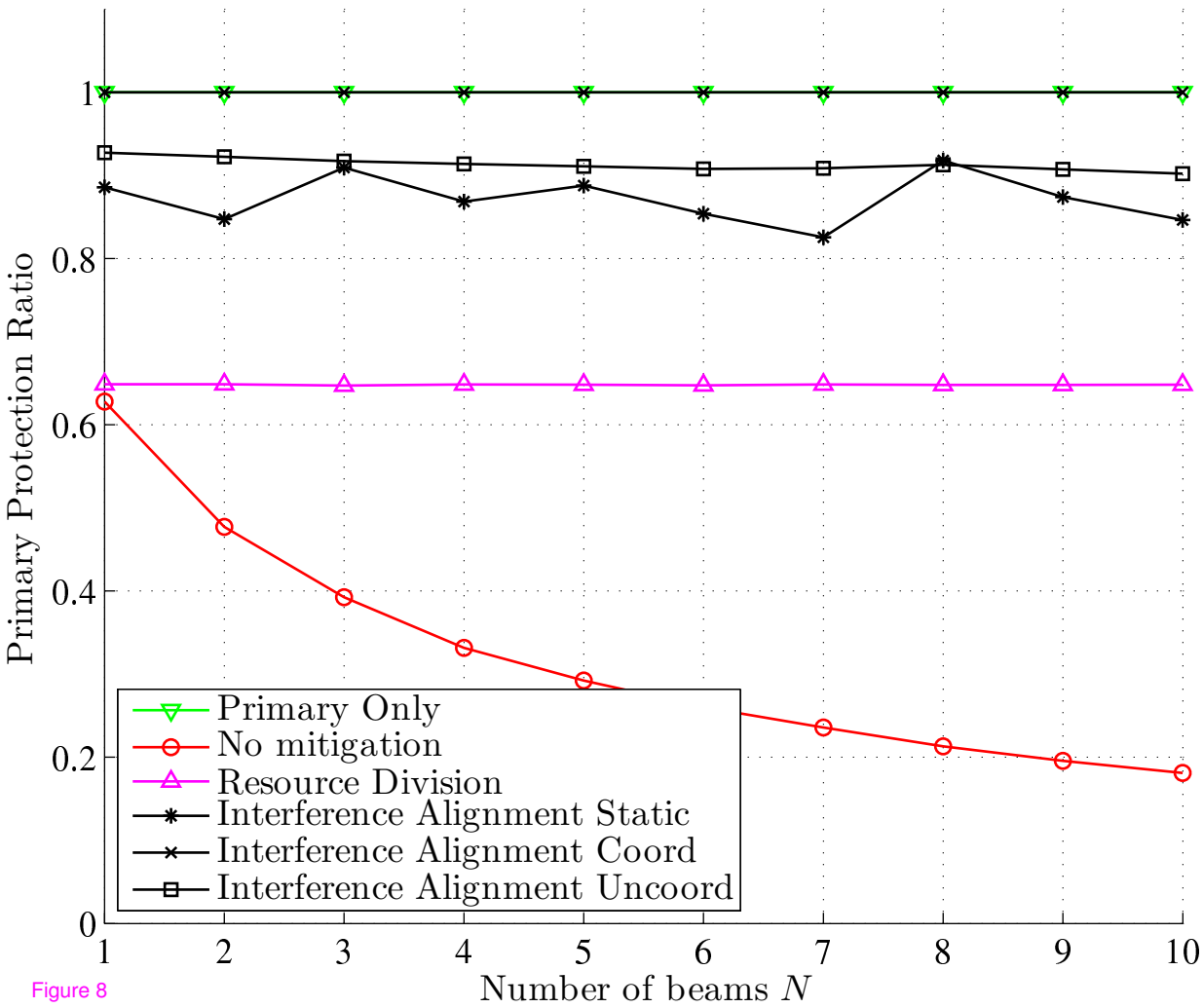


Figure 8